Current Biology 22, 1500–1505, August 21, 2012 ©2012 Elsevier Ltd All rights reserved http://dx.doi.org/10.1016/j.cub.2012.06.025

Report

Tropomodulin Protects α-Catenin-Dependent Junctional-Actin Networks under Stress during Epithelial Morphogenesis

Elisabeth A. Cox-Paulson,[1] Elise Walck-Shannon,[2] Allison M. Lynch,[3] Sawako Yamashiro,[4,5] Ronen Zaidel-Bar,[3,6] Celeste C. Eno,[2] Shoichiro Ono,[4] and Jeff Hardin[2,3,*]

[1]Department of Biology, State University of New York at Geneseo, 353 Integrated Science Center, 1 College Circle, Geneseo, NY 14454, USA

[2]Program in Genetics, University of Wisconsin–Madison, 1117 W. Johnson Street, Madison, WI 53706, USA

[3]Department of Zoology, University of Wisconsin–Madison, 1117 W. Johnson Street, Madison, WI 53706, USA

[4]Department of Pathology, Emory University, Whitehead Research Building, Room 105N, Atlanta, GA 30322, USA

Summary

α-catenin is central to recruitment of actin networks to the cadherin-catenin complex [1, 2], but how such networks are subsequently stabilized against stress applied during morphogenesis is poorly understood. To identify proteins that functionally interact with α-catenin in this process, we performed enhancer screening using a weak allele of the *C. elegans* α-catenin, *hmp-1*, thereby identifying UNC-94/tropomodulin. Tropomodulins (Tmods) cap the minus ends of F-actin in sarcomeres [3]. They also regulate lamellipodia [4], can promote actin nucleation [5], and are required for normal cardiovascular development [6, 7] and neuronal growth-cone morphology [8]. Tmods regulate the morphology of cultured epithelial cells [9], but their role in epithelia in vivo remains unexplored. We find that UNC-94 is enriched within a HMP-1-dependent junctional-actin network at epidermal adherens junctions subject to stress during morphogenesis. Loss of UNC-94 leads to discontinuity of this network, and high-speed filming of *hmp-1(fe4);unc-94(RNAi)* embryos reveals large junctional displacements that depend on the Rho pathway. In vitro, UNC-94 acts in combination with HMP-1, leading to longer actin bundles than with HMP-1 alone. Our data suggest that Tmods protect actin filaments recruited by α-catenin from minus-end subunit loss, enabling them to withstand the stresses of morphogenesis.

Results and Discussion

C. elegans epidermal morphogenesis provides an excellent context in which to investigate the relationship between actin and α-catenin in vivo. The embryonic epidermis contains three types of cells: (1) dorsal cells, which eventually fuse into a syncytium; (2) lateral (seam) cells, arranged in a single row along the anterior-posterior axis on each side of the embryo; and (3) ventral cells. A conserved cadherin-catenin complex (CCC), including HMR-1/cadherin, HMP-2/β-catenin, HMP-1/α-catenin, and JAC-1/p120-catenin [10, 11], is crucial for epidermal morphogenesis [12, 13]. Actomyosin-mediated contractile stresses are transmitted by circumferential actin filament bundles (CFBs) in dorsal and ventral epidermal cells. CFBs insert orthogonally at junctional boundaries between lateral epidermal cells and dorsal and ventral epidermal cells and help to drive the 4-fold elongation of the embryo. CFB anchorage at adherens junctions (AJs) requires the CCC [14–16].

Functional interactions between multiple pathways are important for both focal adhesions and hemidesmosomes [17, 18]. However, a systematic search for similar functional interactions has not been carried out for AJs. We performed such a search, using feeding RNA interference (RNAi) against genes on chromosome I to find lethal enhancers of a weak loss-of-function allele of *hmp-1*, *fe4*. *hmp-1(fe4)* mutants exhibit embryonic and early larval lethality; escapers develop into fertile adults that have body-shape defects [11]. The *fe4* lesion results in an amino-acid substitution in the VH3 domain of HMP-1 [11], which slightly weakens F-actin binding (S. Maiden and J.H., unpublished data).

We identified several genes implicated in regulating cell-cell adhesion, including the AF6/Afadin ortholog (*afd-1*) and an exocyst component (*sec-8*) [19–21], validating our approach. A full analysis, including results for the other five chromosomes, will be published elsewhere (A.M.L. et al., unpublished data). Among the enhancers was UNC-94, a tropomodulin (Tmod) family member.

To examine the functional relationship between HMP-1 and UNC-94, we first performed four-dimensional Nomarski microscopy on *hmp-1(fe4);unc-94(RNAi)* embryos (Figure 1A). Wild-type embryos elongated to approximately 4-fold their initial length before hatching. *unc-94(RNAi)* embryos appeared superficially wild-type, even though *unc-94(RNAi)* lowered UNC-94 protein to virtually undetectable levels (Figure S1A available online). *hmp-1(fe4)* embryos exhibited defective elongation (Figure 1A) and approximately 80% died as embryos and L1 larvae (n = 95). *hmp-1(fe4)* embryos that hatched typically elongated to only twice their original length and had severe body-shape defects. In contrast, 100% of *hmp-1(fe4);unc-94(RNAi)* embryos exhibited embryonic lethality (n = 93). Of these, 95% failed to elongate past the 1.5-fold stage, and they then retracted to their original body length (Figure 1A), compared with only 13% of *hmp-1(fe4)* embryos (see Movie S1 for movies of representative embryos). Thus, HMP-1 and UNC-94 together are essential for epidermal elongation.

Second, we performed immunostaining with an antibody that we previously used to show that UNC-94 is found at body wall-muscle cell-cell boundaries and at the minus ends of sarcomeric thin filaments [22, 23]. UNC-94 was first detectable at the 2-fold stage and was enriched at seam-ventral and seam-dorsal cell borders, the same borders where CFBs transmit stress during elongation (Figure 1B; see Figure 1C for the relationship between CFBs and junctional actin in a wild-type embryo). Although UNC-94 is near AJs, it is distal

[5]Present address: Laboratory of Single-Molecule Cell Biology, Tohoku University Graduate School of Life Sciences, 6-3 Aoba, Aramaki-Aza, Aoba-ku, Sendai, Miyagi 980-8578, Japan

[6]Present address: Mechanobiology Institute Singapore, T-Lab, 5A Engineering Drive 1, National University of Singapore, Singapore 117411, Singapore

*Correspondence: jdhardin@wisc.edu

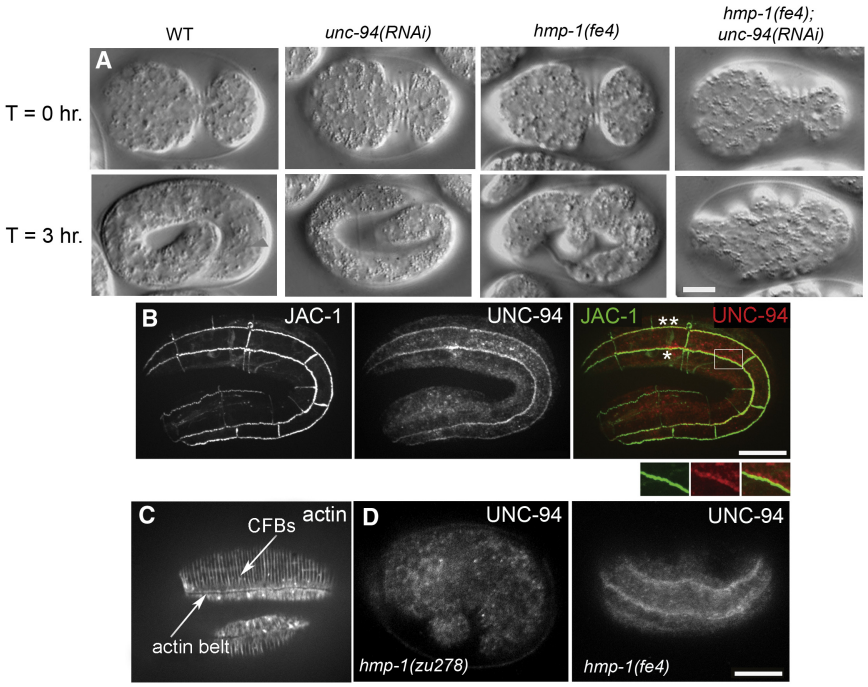

Figure 1. *hmp-1(fe4);unc-94(RNAi)* Embryos Arrest during Embryonic Elongation, and Epidermal UNC-94 Localization to Junctions Requires *hmp-1* Function

(A) Nomarski images of representative embryos undergoing elongation are shown at the indicated time intervals. Embryos are initially oriented with the anterior to the left and the ventral side up at time (T) = 0 hr, and lateral views are shown for all other time points. T = 0 hr shows embryos at the completion of enclosure. Wild-type (WT), *unc-94(RNAi)*, *hmp-1(fe4)*, and *hmp-1(fe4);unc-94(RNAi)* embryos are shown. No obvious defects in elongation are evident in the *unc-94(RNAi)* embryo. *hmp-1(fe4)* embryos develop mild body-shape defects during elongation. 95% of *hmp-1(fe4);unc-94(RNAi)* embryos (n = 93) elongate to the 1.5-fold stage or less, then retract to their original length. See Movie S1.

(B) Wild-type embryo expressing JAC-1::GFP to mark AJs and stained with an affinity-purified rabbit UNC-94 antibody. Seam-ventral (*) and seam-dorsal (**) cell borders are indicated. UNC-94 is first detected at epidermal-cell borders around the 2-fold stage of elongation. The color merge shows JAC-1::GFP in green and UNC-94 in red. Enlargement of the boxed region shows UNC-94 staining overlapping JAC-1::GFP.

(C) Wild-type stained with phalloidin. CFBs and the junctional-actin belt are indicated.

(D) UNC-94 staining in wild-type and *hmp-1* mutants. In wild-type elongation-stage embryos, 23% have UNC-94 localization at epidermal-cell borders (n = 79). In *hmp-1(zu278)* embryos, 0% have UNC-94 localization at epidermal-cell borders (n = 87). In *hmp-1(fe4)* embryos, 35% have UNC-94 localization at epidermal-cell borders (n = 63). Note that this staining was done via freeze-cracking, which is known to disrupt actin but preserves the UNC-94 epitope recognized by UNC-94 antibodies. Disruption of junctional actin caused by this technique may account for the percentage of embryos exhibiting UNC-94 localization at epidermal-cell borders. Bars represent 10 μm.

to them and extends into the cytoplasm, in the same location as the junctional-actin band that runs parallel to AJs. Consistent with this localization pattern, UNC-94 did not coimmunoprecipitate with HMP-1 under conditions in which HMP-1 and HMP-2 did (Figure S1B). Significantly, UNC-94 did not localize to epidermal junctions in *hmp-1(zu278)* homozygotes, which produce a truncated HMP-1 protein incapable of binding actin [16] (Figure 1D), indicating that HMP-1's actin-binding activity is required for mobilization of actin filaments containing UNC-94 near epidermal-cell borders. In contrast, UNC-94 largely localized normally to epidermal-cell borders in *hmp-1(fe4)* embryos (Figure 1D) and localized in pharyngeal cells in a HMP-1-independent manner (Figure S1C). Thus, HMP-1 acts upstream of UNC-94 at epidermal-cell borders normally under tension, but this functional relationship is not mediated through direct physical binding.

To better understand why *hmp-1(fe4);unc-94(RNAi)* embryos fail to elongate, we covisualized AJs and actin during this process using phalloidin staining and JAC-1/p120-catenin::GFP. Strikingly, seam-dorsal and seam-ventral epidermal-cell borders in *hmp-1(fe4);unc-94(RNAi)* embryos were highly disrupted, appearing ripped apart and yielding a characteristic zigzag pattern (Figure 2A). Junctions between other epidermal cells were no more perturbed than those in *hmp-1(fe4)* homozygotes. In areas of perturbed JAC-1::GFP, only some faint actin filaments were visible. Despite this, CFBs were still present in *hmp-1(fe4);unc-94(RNAi)* embryos, interfacing with the edges of the mislocalized JAC-1::GFP (Figure 2A). The junctional-actin belt was still present but was more diffuse in *hmp-1(fe4);unc-94(RNAi)* embryos compared to *hmp-1(fe4)* (Figure 2A, black arrows). The perturbed AJs and actin organization at these epidermal-cell borders in *hmp-1(fe4);unc-94(RNAi)* embryos probably account for their failed elongation.

Immunostaining experiments demonstrated that HMR-1 colocalized with mislocalized JAC-1::GFP in *hmp-1(fe4);unc-94(RNAi)* embryos, indicating that the entire CCC was affected (Figure 2B, top). In contrast, AJM-1, a component of the more basal AJM-1/DLG-1 complex, was unaffected in *hmp-1(fe4);unc-94(RNAi)* embryos (Figure 2B, bottom). Thus, UNC-94 specifically regulates the CCC and its associated actin.

To better characterize the range of defects in *unc-94(tm724)* and *unc-94(RNAi)* embryos, we scored wild-type and *unc-94* loss-of-function embryos stained with phalloidin based on the extent of F-actin disruption (Figure S2). We found defects in both junctional actin and CFBs, suggesting that UNC-94 has a role not only in maintaining proper junctional actin, but also in the anchoring of CFBs to the junctional-actin band. To examine junctional-proximal actin defects in more detail, we measured the extent to which junctional actin was contiguous at seam-dorsal and seam-ventral boundaries in wild-type and *unc-94(tm724)* embryos using phalloidin staining (Figures 2C and 2D). In wild-type embryos, 73.7 ± 2.7% (mean ± SEM; n = 11 cells) of the junctional perimeter contained signal, compared with 48.9 ± 4.2% in *unc-94(tm724)* embryos (n = 16 cells; significantly different, $p < 0.0002$, heteroscedastic t test). Similarly, the mean length of contiguous regions of actin at junctions was significantly greater in wild-type embryos (0.41 ± 0.11 μm, n = 11 cells) versus *unc-94(tm724)* embryos (0.13 ± 0.02 μm, n = 16 cells; significantly different, $p < 0.04$). Such defects may have a common cause: defects in the junctional-actin band may affect proper anchoring and/or spacing

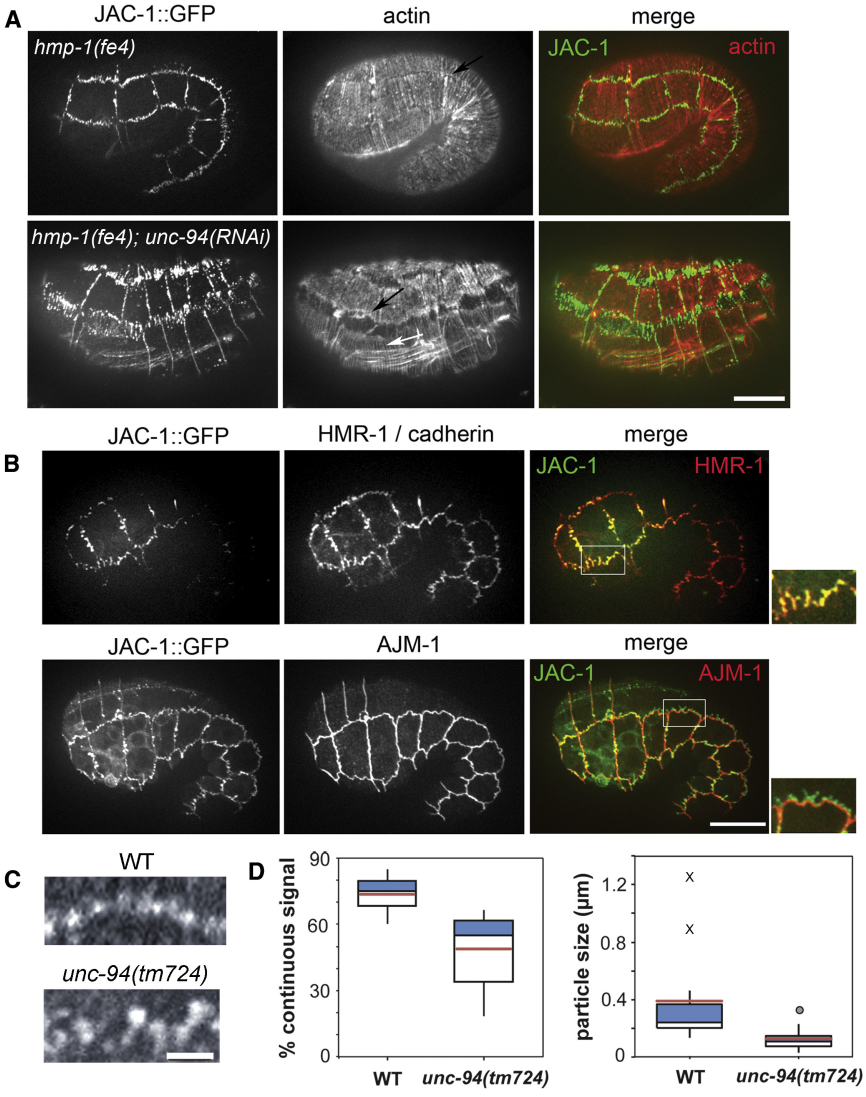

Figure 2. UNC-94 Contributes to AJ Stability

(A) Representative *hmp-1(fe4)* and *hmp-1(fe4);unc-94(RNAi)* embryos. Embryos are of similar age (the *hmp-1(fe4);unc-94(RNAi)* embryo has retracted). Embryos express JAC-1/p120catenin::GFP and are stained with phalloidin for visualization of actin. Color merges show JAC-1::GFP in green and actin in red. In *hmp-1(fe4);unc-94(RNAi)* embryos, JAC-1::GFP is fragmented and mislocalized at seam-dorsal and seam-ventral borders. Actin is depleted in areas of disrupted JAC-1::GFP; however, CFBs (white arrow) and diffuse junctional actin (black arrow) are still visible. The anterior is to the left in all panels. Bar represents 10 μm.

(B) In *hmp-1(fe4);unc-94(RNAi)* embryos, the CCC is selectively perturbed. Prearrest *hmp-1(fe4);unc-94(RNAi)* embryos expressing JAC-1::GFP were stained for either HMR-1/cadherin or AJM-1. Color merges show that HMR-1 (red) colocalizes with JAC-1::GFP (green), and that AJM-1 is not perturbed in regions where JAC-1::GFP is mislocalized. For all images in (A)–(D), anterior is to the left.

(C) Junctional-proximal actin in representative wild-type (WT; top) and *unc-94(tm724)* embryos (bottom). Regular puncta of actin are connected along the junction in wild-type embryos, but gaps are present in junctions from *unc-94(tm724)* embryos. Bars represent 10 μm.

(D) Box plots of the total percentage of junctional area in which actin signal is present (left) and the average length of contiguous regions of actin (right). Blue: First quartile; white: third quartile; pink: mean. The circle represents a mild outlier; X represents extreme outliers. In wild-type, there are occasional stretches of long, unbroken domains of positive signal along entire cells or multiple cells (X).

of CFBs. Vertebrate Tmod3 may similarly stabilize F-actin at lateral cell membranes in immortalized epithelial-cell lines [9].

Taken together, these data suggest an important role for HMP-1 and UNC-94 in regulation of AJs and junctional actin at cell borders under stress during morphogenesis. Next, we observed CCC dynamics in living, prearrested embryos in *jac-1::gfp*-expressing embryos using high-speed filming (Figures 3A–3C). In wild-type embryos, JAC-1::GFP was restricted to the apicolateral contact zones between epidermal cells (Figure 3A). *unc-94(RNAi)* and *unc-94(tm724)* embryos exhibited JAC-1::GFP dynamics similar to wild-type, though rarely some mislocalization occured (Figures S3A and S3B). In *hmp-1(fe4)* homozygotes, the JAC-1::GFP distribution was slightly fragmented, and some JAC-1::GFP was transiently pulled away from the main area of the junction (Figure 3B). Strong zygotic loss of *hmp-1* function in *zu278* homozygotes yielded a similar mild effect (Figure S3C), consistent with our previous report [24]. In contrast to single mutants, however, dislocation of JAC-1::GFP was greatly enhanced in *hmp-1(fe4);unc-94(RNAi)* embryos (Figure 3C). Reslicing images through the z axis of these extended regions showed that they are linear and occur perpendicular to the AJ (data not shown). Their spacing and linearity is consistent with them being caused by pulling forces exerted by the CFBs. *hmp-1(fe4);unc-94(RNAi)* embryos formed about twice as many JAC-1::GFP extensions (≥0.5 μm long) as *hmp-1(fe4)* embryos (Figure 3D). Moreover, as demonstrated in Figure 2C, the AJs of *hmp-1(fe4);unc-94(RNAi)* embryos became progressively more disrupted as time goes on, suggesting that applied stress results in dystrophic disruption of these junctions. Significantly, these regions extended into both seam and ventral or dorsal epidermal cells, with many more in the latter (Table S1). Tissue-specific rescue experiments further demonstrated that although UNC-94 plays a role in both seam cells and nonseam cells, there is a more stringent requirement in nonseam cells (Figure S4A).

The phenotypes we observed are very similar to those described previously in *rga-2*/RhoGAP mutants [25], though they are less pervasive along the apicobasal axis. We therefore assessed whether reducing stress on epidermal junctions could ameliorate the JAC-1::GFP extensions observed in *hmp-1(fe4);unc-94(RNAi)* embryos, using RNAi against *let-502/Rho kinase*. *hmp-1(fe4);unc-94;let-502(RNAi)* embryos exhibited a significant decrease in the number of JAC-1::GFP extensions (Figure 3D), and arrested embryos showed less JAC-1::GFP mislocalization (cf. Figure S3D versus Figure S3E). This suggests that the AJs in *hmp-1(fe4);unc-94(RNAi)*

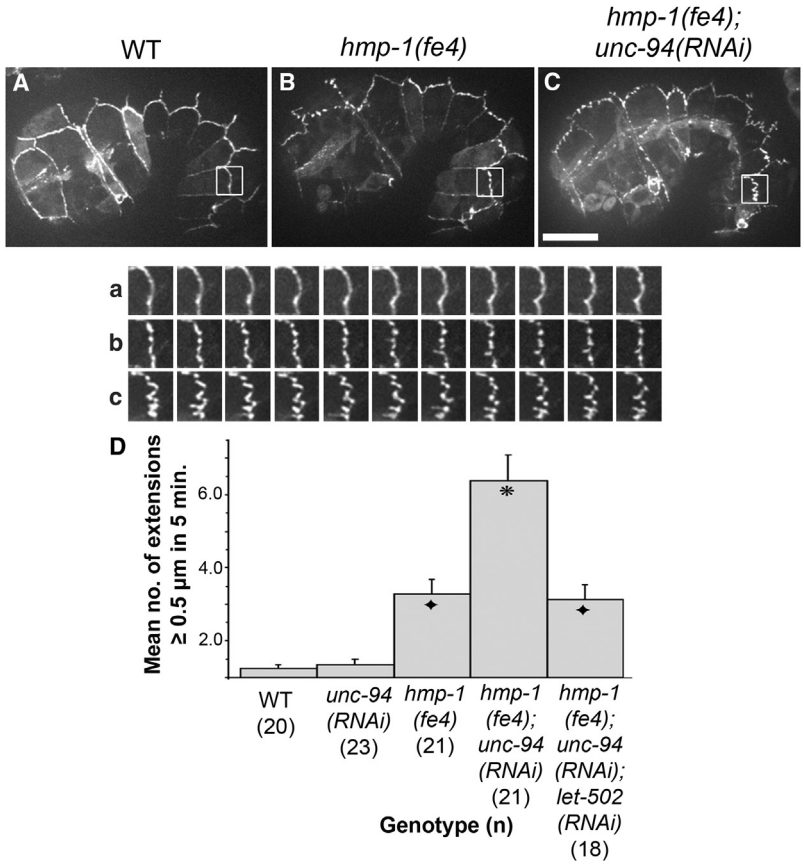

Figure 3. AJs of *hmp-1(fe4);unc-94(RNAi)* Embryos Exhibit Abnormal Dynamics

(A)–(C) Images from spinning-disk confocal movies of embryos expressing JAC-1::GFP are shown. (a)–(c) show an enlargement of the boxed regions in (A)–(C) at 30 s intervals for 5 min. Movie S2 corresponds to (a)–(c). In wild-type embryos (A), JAC-1::GFP localizes to epidermal-cell borders; in *hmp-1(fe4)* embryos (B), there are occasional areas in which JAC-1::GFP is transiently extended away from its normal position. In *hmp-1(fe4);unc-94(RNAi)* embryos (C), this behavior is more pronounced. Bar represents 10 μm.

(D) Bar graph showing quantification of the number (mean ± SEM; n indicated in parentheses) of JAC-1::GFP extensions longer than 5 μm formed at either the seam-dorsal or seam-ventral cell border during 5 min of filming. Embryos at comma to 1.5-fold stage were scored. Each extension was measured only once, at its longest length. Asterisk: significantly different from *hmp-1(fe4)* and *hmp-1(fe4);unc-94(RNAi);let-502(RNAi)* (Tukey test: $p < 0.01$). Black diamonds: not significantly different from *hmp-1(fe4)* ($p > 0.5$).

embryos are not able to withstand the stress transmitted by CFBs during elongation and instead become pulled in the direction of the exerted force. To further investigate the effects of *let-502* loss of function on junctions, we used a temperature-sensitive *let-502* mutant to assess whether LET-502 activity is required for recruitment of UNC-94 to cell borders and found that this is not the case, although cell elongation along the anterior-posterior axis is required for compaction of the zone of UNC-94 expression along seam-nonseam borders (Figure S4B).

To gain mechanistic insight into how HMP-1 and UNC-94 act together to modulate actin networks, we performed in vitro actin-binding and -bundling assays. We showed previously that UNC-94 alone can inhibit latrunculin A-induced depolymerization of plus end-capped *C. elegans* F-actin and that UNC-94 blocks minus-end F-actin depolymerization induced by UNC-60B/ADF-cofilin [23]. We also showed previously that full-length HMP-1 alone can cosediment with actin filaments in vitro. This activity appears to be regulated by intramolecular interactions within the full-length protein, given that the full-length protein cosediments less avidly than C-terminal fragments [16]. We therefore examined the combined effects of HMP-1 and UNC-94 on actin-filament morphology in vitro using fluorescently labeled actin filaments capped at the plus ends by CapZ, to which HMP-1, UNC-94, or both were added (Figure 4A). Added alone, HMP-1 induced actin bundles, as did other α-catenins [26–28]. However, actin bundles generated in the presence of both HMP-1 and UNC-94 (n = 603, average length = 6.1 μm ± 2.7 SD) were 42% longer than those resulting from HMP-1 alone (n = 663, average length = 4.3 μm ± 2.8; significantly different, $p < 0.001$, Figure 4B), and this increase is due in part to an increase in long bundles (Figure 4B, bracket). Taken together, these data indicate that HMP-1 and UNC-94 probably act together to generate robust actin filaments in the junctional-actin band, which in turn resist mechanical deformation due to Rho-mediated actomyosin contractility.

The actin cytoskeleton and AJs cooperate to drive numerous epithelial morphogenetic events [2]. AJs recruit actin via α-catenin; initial recruitment may be modulated by Arp2/3-mediated actin branching or by processive plus-end proteins that stimulate more linear networks [2]. Once actin networks form at AJs, however, they must withstand stress and resist dissolution. Our results indicate a new role for Tmod at the minus ends of actin filaments in this process.

In the embryonic epidermis of *C. elegans*, UNC-94 is enriched at a subset of epidermal-cell borders that interface with CFBs, within the dense network of junctional-actin bundles that runs lateral to AJs at these cell borders. Our in vitro analysis indicates that UNC-94 can protect filaments bundled by HMP-1 from minus-end subunit loss, because this assay was performed under conditions that favor depolymerization from the minus end rather than addition of monomers to plus ends. Because some Tmods promote actin nucleation [5], a non-mutually exclusive possibility is that UNC-94 also plays a supporting role in de novo formation of junctional-actin filaments.

In *hmp-1(fe4);unc-94(RNAi)* embryos, inefficient actin recruitment by mutant α-catenin, coupled with minus-end subunit loss, may lead to a less robust junctional-actin network, which in turn results in lateral instability of AJs. If CFBs are mechanically coupled to the junctional-actin band near their tips (e.g., via actin-crosslinking proteins or through α-catenin itself), stress will tend to be distributed laterally throughout the junctional-actin band, reducing stress at CFB-insertion sites. We envision such reinforcement as functioning in much the same way that the roots of a tree protect it from being uprooted: by distributing stress laterally. This idea is supported by our observation that decreasing actomyosin contractility alleviates the junctional displacements

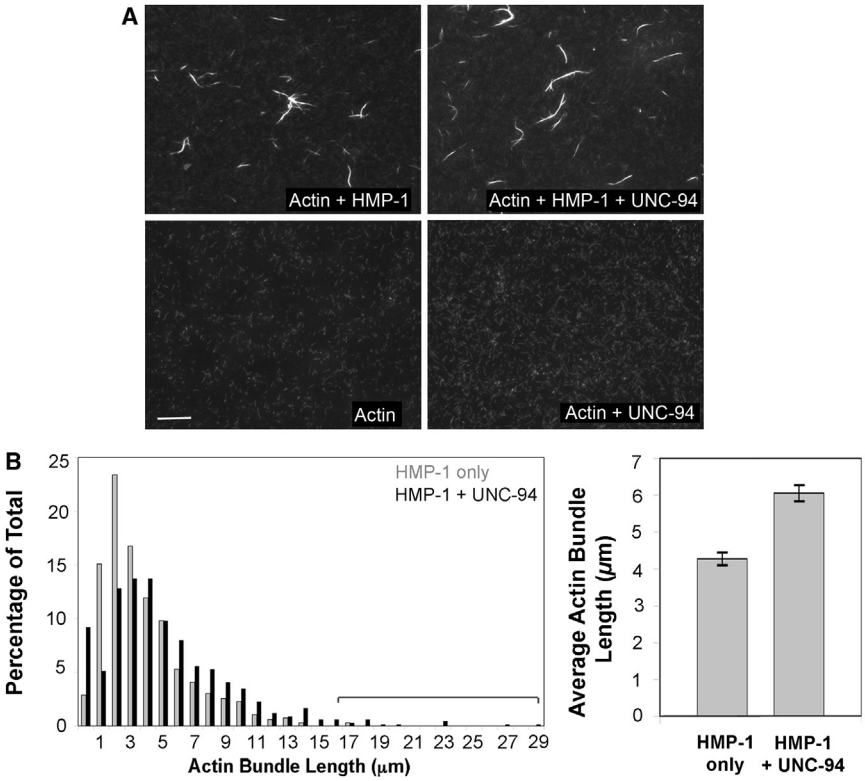

Figure 4. HMP-1 and UNC-94 Synergistically Regulate Actin Bundles In Vitro

(A) Images show fluorescently labeled, plus end-capped F-actin (5 μM), to which either HMP-1 (5 μM), UNC-94 (2.5 μM), or both have been added. Note that actin bundles form only when HMP-1 is present and that UNC-94 can lengthen HMP-1-generated actin bundles. Bar represents 10 μm.

(B) (Left) Histogram of actin-bundle length when HMP-1 is added alone (n = 663) or together with UNC-94 (n = 603). Percentage of bundles exhibiting particular lengths (indicated in μm) is shown. The bracket indicates that when HMP-1 and UNC-94 are added together, there is an increase in the longest population of bundled filaments. (Right) Mean length of actin bundles formed by HMP-1 alone and HMP-1 plus UNC-94. Error bars represent SEM. Actin bundles generated by HMP-1 plus UNC-94 are significantly longer than those generated by HMP-1 alone ($p < 0.001$, two-tailed t test).

observed in *hmp-1(fe4);unc-94(RNAi)* embryos. We propose that the retraction phenotype exhibited by *hmp-1(fe4);tmd-1(RNAi)* embryos (in which the embryos extend to ~1.5-fold and then retract to their original length) may be due to a combination of uneven CFB-pulling forces from abnormally arranged CFBs and weakened ultrastructure of the junctional-actin band. This could result in failure to translate the stress applied by CFBs into the epidermal cell-shape changes that drive elongation.

Junctional-actin bands are present in many epithelial-cell types. The forces applied to them can be aligned predominantly along the junction or orthogonal to it, the latter being the case during *C. elegans* embryonic elongation (reviewed in [29]). Our work suggests that regulation of minus-end actin dynamics via Tmod plays an important role in promoting stability of actin networks under this orthogonal stress. Future experiments aimed at teasing apart the ultrastructure and biochemical regulation of junctional-actin bands should help to clarify their function, as well as how multiple actin regulators contribute to the mechanical integrity of AJs.

Supplemental Information

Supplemental Information includes four figures, one table, two movies, and Supplemental Experimental Procedures and can be found with this article online at http://dx.doi.org/10.1016/j.cub.2012.06.025.

Acknowledgments

We thank Yuji Kohara for providing complementary DNA, Shohei Mitani for providing the *unc-94(tm724)* allele, Ryan King and the Ivan Rayment lab for technical assistance in expression and purification of His-tagged UNC-94, and Michael Joyce for help with coimmunoprecipitation assays. We thank Vida Praitis and Bill Bement for critical reading of the manuscript and Theresa Grana for helpful comments. This work was supported by National Institutes of Health (NIH) grants NRSA GM067410 and R15 HD059952 to E.A.C.-P.; NIH grant R01 GM58038, Muscular Dystrophy Association grant 4218, and National Science Foundation grant IOB 0518081 to J.H., and NIH grant R01 AR48615 to S.O.

Received: November 17, 2011
Revised: April 9, 2012
Accepted: June 6, 2012
Published online: July 5, 2012

References

1. Weis, W.I., and Nelson, W.J. (2006). Re-solving the cadherin-catenin-actin conundrum. J. Biol. Chem. *281*, 35593–35597.
2. Niessen, C.M., Leckband, D., and Yap, A.S. (2011). Tissue organization by cadherin adhesion molecules: dynamic molecular and cellular mechanisms of morphogenetic regulation. Physiol. Rev. *91*, 691–731.
3. Fischer, R.S., and Fowler, V.M. (2003). Tropomodulins: life at the slow end. Trends Cell Biol. *13*, 593–601.
4. Littlefield, R.S., and Fowler, V.M. (2008). Thin filament length regulation in striated muscle sarcomeres: pointed-end dynamics go beyond a nebulin ruler. Semin. Cell Dev. Biol. *19*, 511–519.
5. Yamashiro, S., Speicher, K.D., Speicher, D.W., and Fowler, V.M. (2010). Mammalian tropomodulins nucleate actin polymerization via their actin monomer binding and filament pointed end-capping activities. J. Biol. Chem. *285*, 33265–33280.
6. Chu, X., Chen, J., Reedy, M.C., Vera, C., Sung, K.L., and Sung, L.A. (2003). E-Tmod capping of actin filaments at the slow-growing end is required to establish mouse embryonic circulation. Am. J. Physiol. Heart Circ. Physiol. *284*, H1827–H1838.
7. Fritz-Six, K.L., Cox, P.R., Fischer, R.S., Xu, B., Gregorio, C.C., Zoghbi, H.Y., and Fowler, V.M. (2003). Aberrant myofibril assembly in tropomodulin1 null mice leads to aborted heart development and embryonic lethality. J. Cell Biol. *163*, 1033–1044.
8. Fath, T., Fischer, R.S., Dehmelt, L., Halpain, S., and Fowler, V.M. (2011). Tropomodulins are negative regulators of neurite outgrowth. Eur. J. Cell Biol. *90*, 291–300.
9. Weber, K.L., Fischer, R.S., and Fowler, V.M. (2007). Tmod3 regulates polarized epithelial cell morphology. J. Cell Sci. *120*, 3625–3632.

10. Costa, M., Raich, W., Agbunag, C., Leung, B., Hardin, J., and Priess, J.R. (1998). A putative catenin-cadherin system mediates morphogenesis of the Caenorhabditis elegans embryo. J. Cell Biol. *141*, 297–308.
11. Pettitt, J., Cox, E.A., Broadbent, I.D., Flett, A., and Hardin, J. (2003). The Caenorhabditis elegans p120 catenin homologue, JAC-1, modulates cadherin-catenin function during epidermal morphogenesis. J. Cell Biol. *162*, 15–22.
12. Cox, E.A., and Hardin, J. (2004). Sticky worms: adhesion complexes in C. elegans. J. Cell Sci. *117*, 1885–1897.
13. Lynch, A.M., and Hardin, J. (2009). The assembly and maintenance of epithelial junctions in C. elegans. Front. Biosci. *14*, 1414–1432.
14. Chisholm, A.D., and Hardin, J. (2005). Epidermal morphogenesis. WormBook, 1–22.
15. Zhang, H., Gally, C., and Labouesse, M. (2010). Tissue morphogenesis: how multiple cells cooperate to generate a tissue. Curr. Opin. Cell Biol. *22*, 575–582.
16. Kwiatkowski, A.V., Maiden, S.L., Pokutta, S., Choi, H.J., Benjamin, J.M., Lynch, A.M., Nelson, W.J., Weis, W.I., and Hardin, J. (2010). In vitro and in vivo reconstitution of the cadherin-catenin-actin complex from Caenorhabditis elegans. Proc. Natl. Acad. Sci. USA *107*, 14591–14596.
17. Zaidel-Bar, R., Itzkovitz, S., Ma'ayan, A., Iyengar, R., and Geiger, B. (2007). Functional atlas of the integrin adhesome. Nat. Cell Biol. *9*, 858–867.
18. Zahreddine, H., Zhang, H., Diogon, M., Nagamatsu, Y., and Labouesse, M. (2010). CRT-1/calreticulin and the E3 ligase EEL-1/HUWE1 control hemidesmosome maturation in C. elegans development. Curr. Biol. *20*, 322–327.
19. Grindstaff, K.K., Yeaman, C., Anandasabapathy, N., Hsu, S.C., Rodriguez-Boulan, E., Scheller, R.H., and Nelson, W.J. (1998). Sec6/8 complex is recruited to cell-cell contacts and specifies transport vesicle delivery to the basal-lateral membrane in epithelial cells. Cell *93*, 731–740.
20. Ikeda, W., Nakanishi, H., Miyoshi, J., Mandai, K., Ishizaki, H., Tanaka, M., Togawa, A., Takahashi, K., Nishioka, H., Yoshida, H., et al. (1999). Afadin: A key molecule essential for structural organization of cell-cell junctions of polarized epithelia during embryogenesis. J. Cell Biol. *146*, 1117–1132.
21. Zhadanov, A.B., Provance, D.W., Jr., Speer, C.A., Coffin, J.D., Goss, D., Blixt, J.A., Reichert, C.M., and Mercer, J.A. (1999). Absence of the tight junctional protein AF-6 disrupts epithelial cell-cell junctions and cell polarity during mouse development. Curr. Biol. *9*, 880–888.
22. Stevenson, T.O., Mercer, K.B., Cox, E.A., Szewczyk, N.J., Conley, C.A., Hardin, J.D., and Benian, G.M. (2007). unc-94 encodes a tropomodulin in Caenorhabditis elegans. J. Mol. Biol. *374*, 936–950.
23. Yamashiro, S., Cox, E.A., Baillie, D.L., Hardin, J.D., and Ono, S. (2008). Sarcomeric actin organization is synergistically promoted by tropomodulin, ADF/cofilin, AIP1 and profilin in C. elegans. J. Cell Sci. *121*, 3867–3877.
24. Simske, J.S., Köppen, M., Sims, P., Hodgkin, J., Yonkof, A., and Hardin, J. (2003). The cell junction protein VAB-9 regulates adhesion and epidermal morphology in C. elegans. Nat. Cell Biol. *5*, 619–625.
25. Diogon, M., Wissler, F., Quintin, S., Nagamatsu, Y., Sookhareea, S., Landmann, F., Hutter, H., Vitale, N., and Labouesse, M. (2007). The RhoGAP RGA-2 and LET-502/ROCK achieve a balance of actomyosin-dependent forces in C. elegans epidermis to control morphogenesis. Development *134*, 2469–2479.
26. Dickinson, D.J., Nelson, W.J., and Weis, W.I. (2011). A polarized epithelium organized by beta- and alpha-catenin predates cadherin and metazoan origins. Science *331*, 1336–1339.
27. Drees, F., Pokutta, S., Yamada, S., Nelson, W.J., and Weis, W.I. (2005). Alpha-catenin is a molecular switch that binds E-cadherin-beta-catenin and regulates actin-filament assembly. Cell *123*, 903–915.
28. Rimm, D.L., Koslov, E.R., Kebriaei, P., Cianci, C.D., and Morrow, J.S. (1995). Alpha 1(E)-catenin is an actin-binding and -bundling protein mediating the attachment of F-actin to the membrane adhesion complex. Proc. Natl. Acad. Sci. USA *92*, 8813–8817.
29. Gomez, G.A., McLachlan, R.W., and Yap, A.S. (2011). Productive tension: force-sensing and homeostasis of cell-cell junctions. Trends Cell Biol. *21*, 499–505.

Current Biology, Volume 22

Supplemental Information

Tropomodulin Protects α-Catenin-Dependent Junctional-Actin Networks under Stress during Epithelial Morphogenesis

Elisabeth A. Cox-Paulson, Elise Walck-Shannon, Allison M. Lynch, Sawako Yamashiro, Ronen Zaidel-Bar, Celeste C. Eno, Shoichiro Ono, and Jeff Hardin

Table S1. Number and Directionality of Junctional Extensions in *hmp-1(fe4)* and *hmp-1(fe4);unc-94(RNAi)* Embryos

	# embryos analyzed	**# total extensions** (>= 0.5 mm)	**# non-seam directed extensions** (>= 0.5 mm)	**# seam directed extensions** (>= 0.5 mm)
hmp-1(fe4); jac-1::gfp	21	48 (2.3 / embryo)	22 (1.0 / embryo)	26 (1.2 / embryo)
hmp-1(fe4); jac-1::gfp; unc-94(RNAi)	18	97 (5.4 / embryo)	60 (3.3 / embryo)	37 (2.1 / embryo)

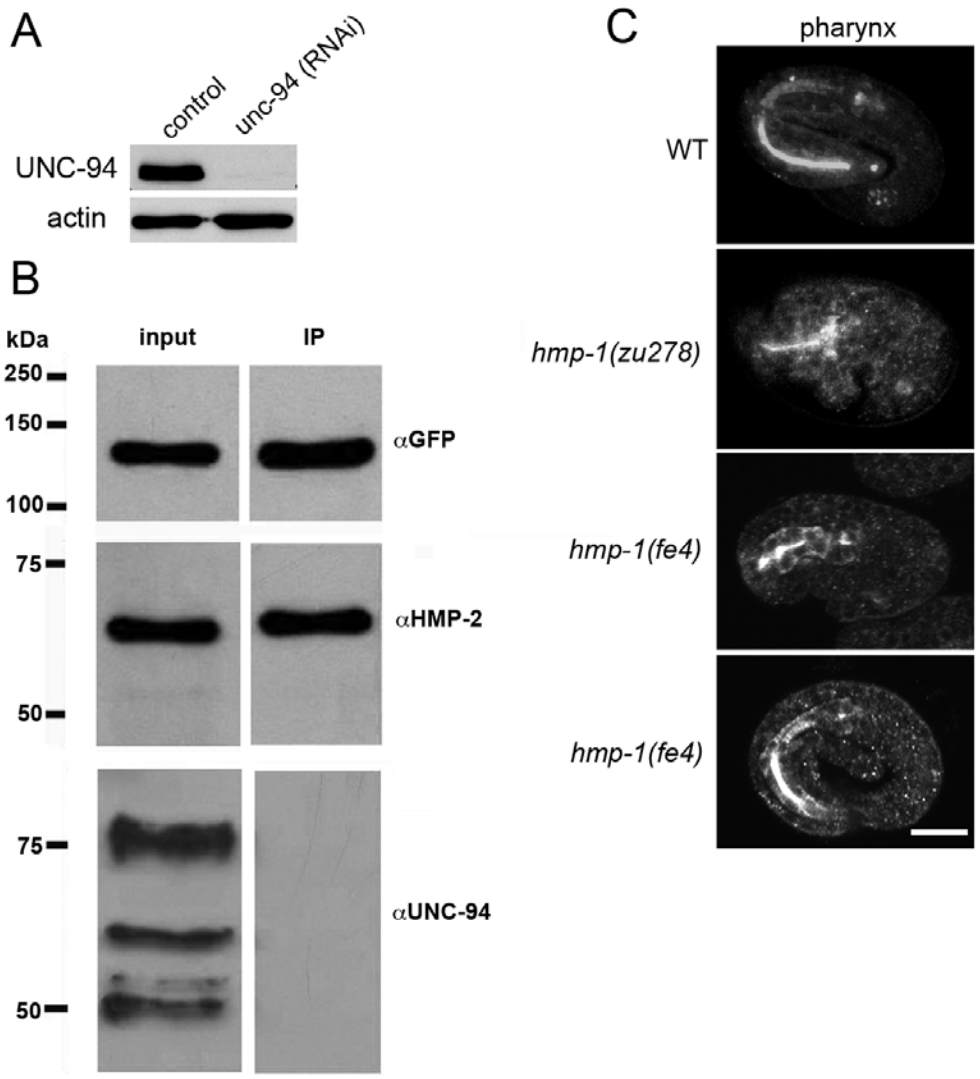

Figure S1. Additional Analysis of HMP-1 and UNC-94 Interactions

A. Western blot showing reduced expression of UNC-94 in *unc-94(RNAi)* embryos. Lysate from 30 N2 or N2; *unc-94(RNAi)* worms was loaded in each lane and probed for either UNC-94 or actin. Western blot showing reduced expression of UNC-94 in embryos treated with *unc-94(RNAi)*. Lysate from 30 N2 or N2; *unc-94(RNAi)* worms was loaded in each lane and probed for either UNC-94 or actin. RNAi was performed via feeding. B. HMP-1 and UNC-94 do not coimmunoprecipitate. SU265 (*hmp-1::gfp; dlg-1::dsRed*) embryos were collected and extracts collected as described in Experimental Procedures. Extracts were subjected to immunoprecipitation using anti-GFP antibodies, and the resulting non-precipitated proteins (input) and immunoprecipitates (IP) were blotted and probed using anti-GFP (αGFP), anti-HMP-2 (αHMP-2), or anti-UNC-94 (αUNC-94) antibodies. Whereas there is robust signal for HMP-1::GFP (top) or HMP-2, a known HMP-1 binding protein (middle) in the IP, there is no detectable UNC-94 (bottom), although there was abundant UNC-94 in the original extract (bottom, left). C. UNC-94 staining in the pharynx. In wild-type elongation-stage embryos, 100% show staining for UNC-94 in the pharynx (n = 79). In *hmp-1(zu278)* embryos, 86% have UNC-94 staining in the pharynx (n = 87). In *hmp-1(fe4)* embryos, 100% of elongating embryos show staining for UNC-94 in the pharynx (n = 63). Bar = 10 μm.

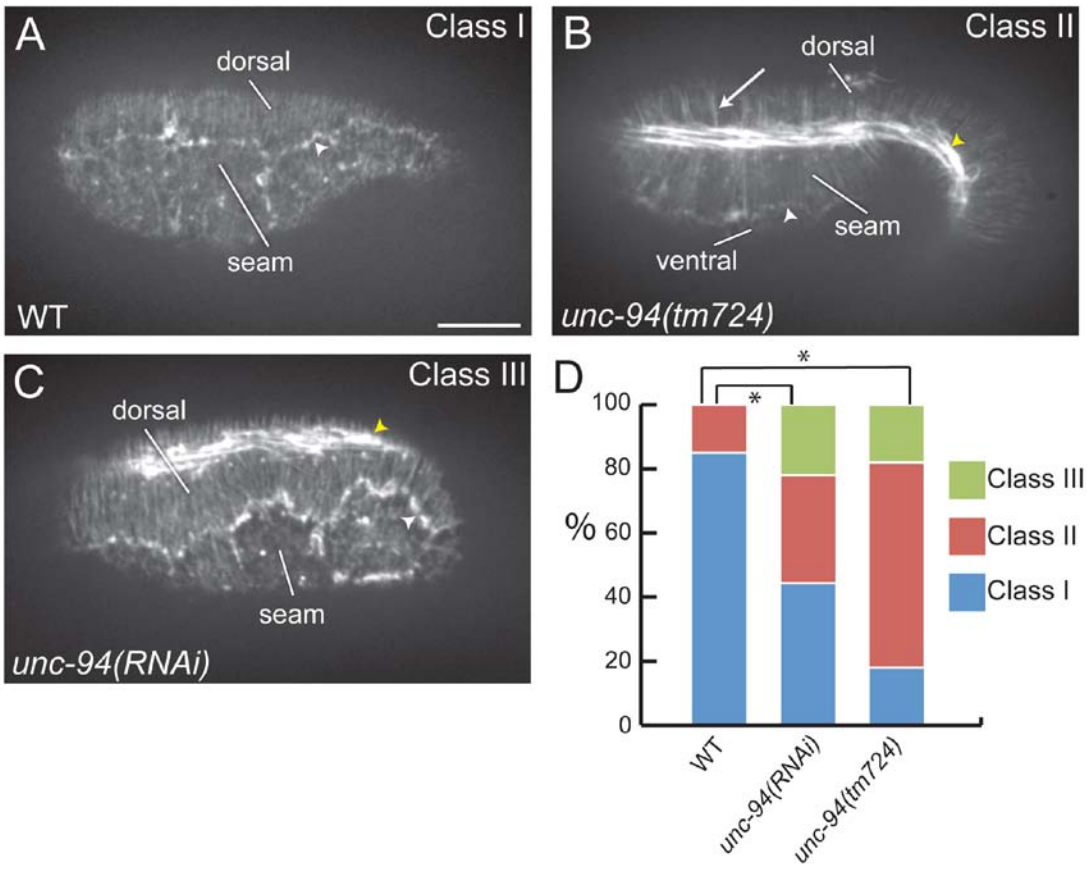

Figure S2. Junctional-Proximal Actin and Circumferential Filament Bundles (CFBs) Are Perturbed in *unc-94* Loss-of-Function Embryos

Phalloidin staining of actin in ~1.5-fold embryos. Phenotypic defects were categorized into three classes. (A) In Class I embryos (wild-type embryo shown), there is a clear thin band of actin at the junction (white arrowhead), evenly spaced CFBs, and a dense meshwork of actin in seam cells. (B) In Class II embryos (*unc-94(tm724)* embryo shown), there are clumps of CFBs (arrow), but the overall amount of actin in the embryo is not decreased. Muscle organization is also perturbed (yellow arrowhead). (C) In Class III embryos (*unc-94(RNAi)* embryo shown), there is clumping of junctional actin and often a substantial decrease in the amount of actin present in seam cells (not visible in this example). As in Class II embryos, muscle organization is perturbed (yellow arrowhead). (D) Distribution of phenotypes for the three genotypes of embryos screened (wildtype, n=13; *unc-94(RNAi)*, n=19; *unc-94(tm724)* n=11). For all images, anterior is to the left; bar=10µm. * = significantly different, $p < 0.05$. *unc-94(RNAi)* and *unc-94(tm724)* are not significantly different ($p = 0.32$).

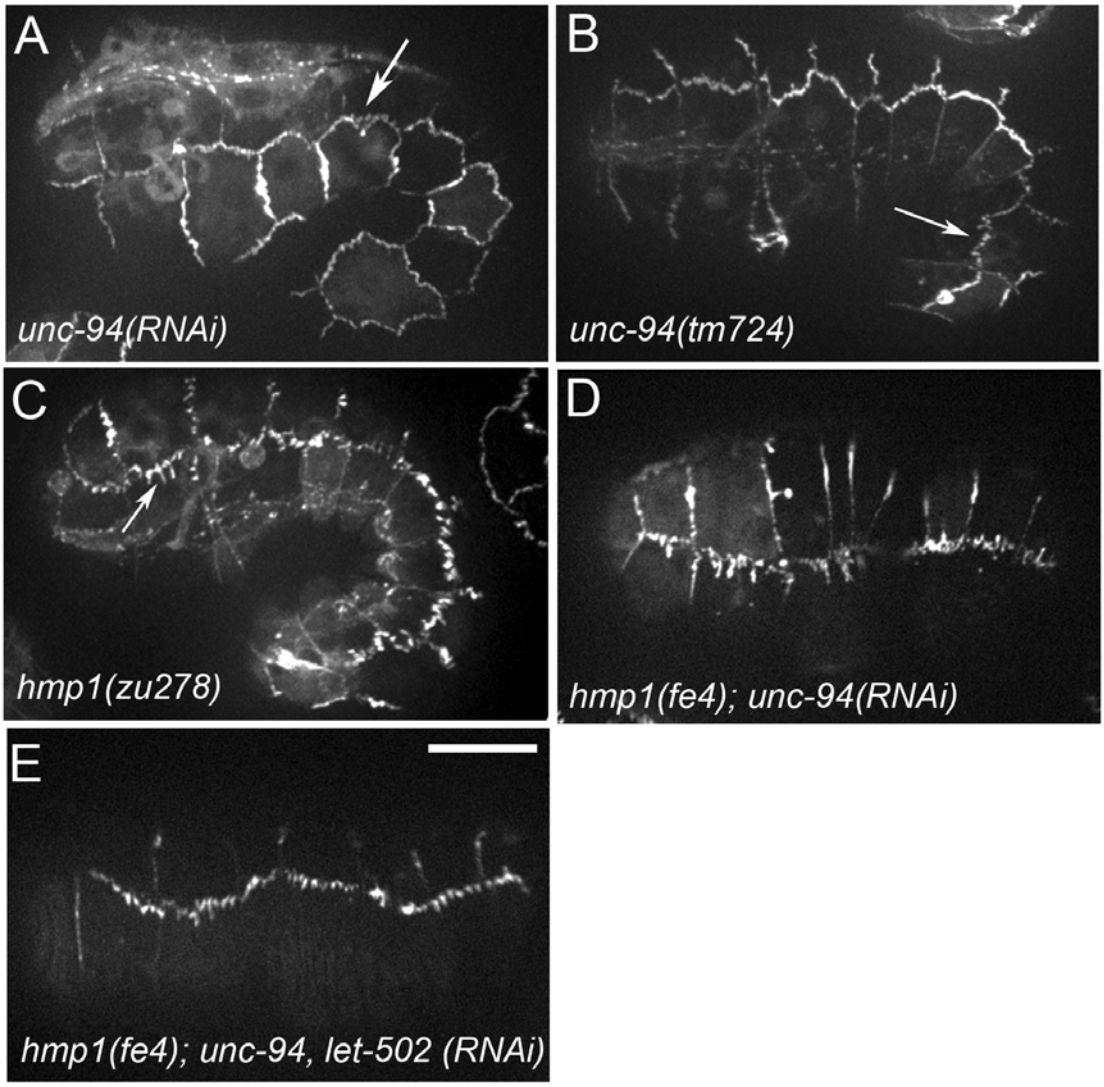

Figure S3. The Adherens Junctions of *hmp-1(fe4);unc-94(RNAi)* Embryos Exhibit Abnormal Dynamics in Living Embryos

JAC-1::GFP localization was assessed in living embryos using spinning disc confocal microscopy. (A, B) *unc-94* loss-of-function results in slightly perturbed adherens junctions. (A) *unc-94(RNAi)* embryo. Regions of JAC-1::GFP mislocalization (arrow), were observed in 3 out of 23 embryos examined. (B) *unc-94(tm724)* embryo. (C) *hmp-1(zu278)* embryo. In 6 out of 6 embryos observed (at the 1.25-1.5 fold stage), the seam:ventral/seam:dorsal borders exhibited dislocation of JAC-1::GFP reminiscent of, but not quite as dynamic as, that seen in *hmp-1(fe4);unc-94(RNAi)* embryos. (D, E) *let-502(RNAi)* ameliorates the junctional dislocation in *hmp-1(fe4);unc-94(RNAi)* embryos. (D) Arrested *hmp-1(fe4);unc-94(RNAi)* embryo showing dislocated JAC-1::GFP. (E) Arrested *hmp-1(fe4);unc-94, let-502(RNAi)* embryo. Some regions in C and D are slightly out of focus due to the shape of the embryos and movement due to muscle twitching. Bar = 10 μm.

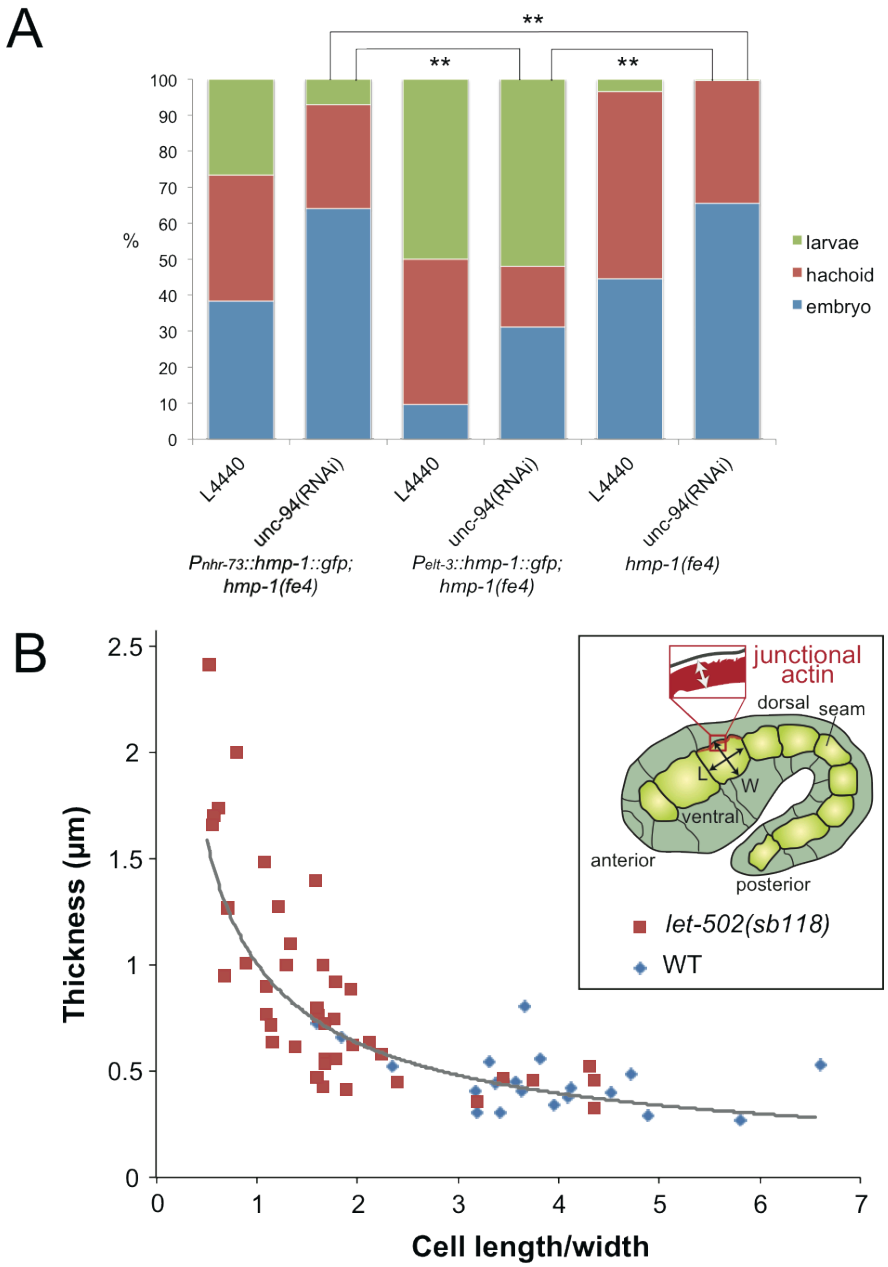

Figure S4. Tissue-Specific Requirements for HMP-1 and UNC-94 Function and Effects of LET-502/ROCK on Junctional-Proximal Actin

A. Tissue-specific rescue of defects in *hmp-1(fe4);unc-94(RNAi)* embryos indicates a major requirement for HMP-1 and UNC-94 in non-seam epidermal cells. *hmp-1(fe4)* hermaphrodites expressing *Pnhr-73::hmp-1::gfp* (expressed in seam cells) or *Pelt-3::hmp-1::gfp* (expressed in non-seam cells) were subjected to *unc-94(RNAi)* via feeding or fed control bacteria (L4440), and progeny scored for developmental arrest. ** = significantly different, $p < 0.001$. B. Loss of *let-502*/Rho kinase function leads to shorter cells with thicker UNC-94-positive junctional proximal actin bands. *let-502(sb118)* embryos were temperature-shifted as described in Experimental Procedures and immunostained for AJM-1(to determine overall cell shape) and UNC-94. The thickness of the UNC-94-containing junctional proximal band was measured as shown and plotted against length/width ratio for *let-502(sb118)* and wild-type embryos. A power curve was used to fit the resulting data.

Supplemental Experimental Procedures

Strains and Alleles

The Bristol N2 strain was used as wildtype. *hmp-1(fe4)* [1] was maintained as a heterozygote over *lon-3(e2175)* as a marker for the wild-type chromosome. The previously described *jac-1::gfp* transgene [1] was integrated via gamma irradiation (*jcIs24*), outcrossed six times, and homozygosed to generate the strain SU295. Crosses were performed to introduce *jcIs24* into *hmp-1(fe4)*/*lon-3(e2175)* and into *unc-94(tm724)*. *unc-94(tm724)* was obtained from Shohei Mitani (National Bioresource Project for *C. elegans*, Tokyo Women's Medical University School of Medicine, Tokyo, Japan). The *unc-94(tm724)* allele has a 695 base pair deletion and 17 bp insertion that might result in a frame shift after the third exon.

A strain (ML753) expressing a *gfp*-tagged fragment of *vab-10* that binds F-actin in epidermal cells (VAB-10(ABD):GFP [2]) was mated with *unc-94(tm724)* or *hmp-1(fe4)* males and the relevant mutation was rehomozygosed to create strains used in spinning disc confocal filming experiments.

HR1157 carries a *let-502* temperature sensitive allele (*sb118*) that was kindly provided by Paul Mains (University of Calgary).

Tissue-specific HMP-1 rescuing constructs were made using Fusion PCR [3]. The *nhr-73* promoter was used for seam-specific expression and the *elt-3* promoter was used for non-seam epidermal expression. Phusion Polymerase (NEB) was used to PCR amplify ~1kb of the *nhr-73* promoter (5' CTTGAGCAACAATTTTCAGAGCAGTGGAGGTTTTGT3' forward and 3'CCATTCGCAGGCAT TCTGAAAATTAATTTTTCTTCAAACTTGCC5' reverse, with 25bp overhang for *hmp-1*) or ~2kb of the *elt-3* promoter (5' ACCGAAATGCCGATGGACATATCAAATGTGAAGACA3' and 3'CATGAGAATTGCCATTCGCAGGCATGAAGTTTGAAATACCAGGTAGCCGA5' reverse, with 25bp overhang for *hmp-1*) from *C. elegans* genomic DNA. *hmp-1::gfp* was PCR amplified using Phusion Polymerase with pJS434 [4] as a template (5' TAATTTTCAGAATGCCTGCGAATGG3' forward and 3' GCATAGTTAAGCCAGCCCCGACACC5' reverse) for fusion to $P_{nhr\text{-}73}$ or 5'ATGTGTCAGAGGTTTTCACCGTCAT3' forward and 3'ATGTGTCAGAGGTTTTCACCGTCAT5' reverse for fusion to Pelt-3). Fusion PCR was performed to connect these two nested PCR products using *Go Taq Long* (for $P_{nhr\text{-}73}$*::hmp-1::gfp*: 5'TATGTGTCAGAGGTTTTCACCGTCAT3' and 3'ATGTGTCAGAGGTTTTCACCGTCAT5'; for $P_{elt\text{-}3}$*::hmp-1::gfp*: 5'GTTTCTACTGTTTCAACATTATGTGTCAGAGGTTTTCACCGTCAT3' and 3'ATGTGTCAGAGGTTTTCACCGTCAT5').

Fusion PCR constructs ($P_{elt\text{-}3}$*::hmp-1::gfp* and P_{nhr73}*::hmp-1::*gfp) were injected into *hmp-1(fe4)* worms. At least two reactions were pooled for injection to minimize the chance of proofreading

errors. About 80ng of the Fusion reactions were co-injected with $P_{ttx\text{-}3}$*::dsRed* into the gonads of *hmp-1(fe4)* worms. Expression of the HMP-1::GFP constructs in either seam or non-seam cells was verified with confocal microscopy.

Antibodies

A polyclonal rabbit anti-UNC-94 antibody was produced and affinity purified by the Proteintech Group, Inc. (Chicago, IL) using amino acids 144-401 of UNC-94b as the antigen as previously described [5]. Rabbit anti-HMR-1 antibody was generously provided by J. Priess (Fred Hutchinson Cancer Research Center, Seattle, WA). MH27 antibodies were purified from ascites fluid (Harlan Sprague Dawley, Madison, WI) from hybridoma cells obtained from the Developmental Hybridoma Bank (Univ. of Iowa). A monoclonal anti-actin antibody (C4, MP Biomedicals, Irvine CA) was used for Western blotting.

Feeding RNAi Screening

The *C. elegans* Chromosome I feeding RNAi library in 96 well format was used for screening [6]. This library contains 2,445 bacterial cultures (HT115 (DE3) strain) each expressing a unique feeding RNAi clone. A starter culture (LB with 25 μg/mL carbenicillin and 12.5 μg/mL tetracycline) was inoculated with a replicator tool, using frozen material from the library plates, and grown overnight at 37^{o}C. A second culture (LB + 25 μg/mL carbenicillin) was inoculated using material from the starter plate and cultured overnight at 37^{o}C. 10 μL of this culture was spread onto triplicate wells of 12 well plates containing Nematode Growth Media [7] supplemented with 25 μg/mL carbenicillin and 1mM isopropyl β-D-thiogalactopyranoside (IPTG). The bacteria were grown overnight to generate a thin lawn.

Approximately 20-30 L3-L4 *hmp-1(fe4)* worms were seeded onto one well for each clone to be tested. After allowing the worms to feed for 24 hours, 8 were singled onto each of the two remaining wells for each clone. After another 24 hours, the worms were removed from the plates. Over the next two days, the wells were visually scanned to determine the approximate percentage of embryonic lethality. Feeding RNAi for wild type worms was performed in a similar manner except that 10-15 worms were seeded in the initial well and four were singled into the duplicate wells. In each round of the screen, *hmp-1(fe4)* worms were fed the empty feeding vector, L4440[8], as a negative control and a feeding vector for the known *hmp-1(fe4)* enhancer, *unc-34* [9] as a positive control.

We identified 44 transcription units that, when depleted with feeding RNAi, enhanced the lethality of *hmp-1(fe4)* to 95% or greater, and yielded less than 12% lethality in wild-type. A

secondary screen was performed to confirm putative enhancers using a different source of double-stranded RNA (dsRNA) and RNAi by injection.

RNAi via Injection and Dead Embryo Counts

dsRNA was injected at 2 μg/μl into one gonad arm per worm, with the exception of *let-502(RNAi)*, which was injected at 1 μg/μl to avoid early arrest due to cytokinesis defects. To score for embryonic and early larval lethality, worms were cultured for 12-16 hours after injection and then singled onto new plates. The embryos produced over the next 24 hours were scored for lethality. To obtain embryos for phenotypic analysis, worms were cut transversely through the vulva at 24 - 30 hours post-injection and extruded embryos were collected.

For tissue-specific rescue experiments, worms were selected for application to either empty vector (L4440) or *tmd-1* feeding RNAi plates based on the dsRed signal. Lethality was counted after 48 hours of feeding. Chi-square analysis was performed using the online contingency table form available at http://www.physics.csbsju.edu/stats/contingency.html.

Morphological Analysis and Embryo Staining

4D Nomarski microscopy was performed as described previously [10]. Phalloidin staining was performed using a modification of a previously described protocol [11]. Briefly, embryos were placed on poly-L-lysine coated slides, aged, treated with 1 mg/ml chitinase in egg salts for 20 min., and fixed with a solution of 4% paraformaldehyde, 0.1 mg/mL lysolecithin, 10 mM EGTA, 48 mM PIPES (pH 6.8), 25 mM HEPES (pH 6.8) and 2 mM $MgCl_2$. Embryos were stained with 1:20 Alexa555-phalloidin (Invitrogen Corp., Carlsbad, CA) overnight at 4^{o}C. For immunostaining, embryos were freeze cracked and stained as described [12] .

For immunocytochemistry experiments and live imaging of JAC-1::GFP and VAB-10(ABD)::GFP, embryos were observed using a Perkin Elmer Ultraview spinning disk confocal microscope and processed as described [9]. For videos of JAC-1::GFP, stacks of images (12-16 sections/stack) were taken at 10 sec intervals for 5 min; for VAB-10(ABD)::GFP, 10-30 focal planes were captured at 30-120 sec intervals. Some images shown are projections of multiple focal planes. Cells in elongating *vab-10(ABD)::gfp* embryos at the comma stage were scored as having discontinuous actin bands if no discernible accumulation of actin could be identified over > 50% of their ventral perimeter.

Actin defects in phalloidin stained specimens were scored as follows. Stained ~1.5-fold embryos were categorized into three classes. In class I embryos a clear, thin band of actin at the junction and evenly spaced circumferential filaments bundles (CFBs) were apparent, along with a dense meshwork

of actin in seam cells. In class II embryos, clumps of CFBs were visible, but the overall amount of actin in the embryo was not decreased. In class III embryos, clumping of junctional actin occurred, and there was a substantial decrease in the amount of actin present in seam cells. Embryos were categorized by three independent assessors and the results compiled. Chi-square analysis was performed as above (see Procedures for tissue-specific rescue).

For measuring continuity of junctional proximal actin networks, a 5 pixel-wide freehand selection was hand-traced along individual cell-cell junctions from maximum-intensity Z stack projections of phalloidin stained specimens. The selection was then straightened using the "Edit->Selection->Straighten…" command in ImageJ. The signal was manually thresholded for each selection using the "Image->Adjust->Threshold…" command to include all visible fluorescence along the straightened cell-cell boundary. The number, size and total area of thresholded particles was then calculated using the "Analyze->Analyze Particles…" command in ImageJ. Since the variances of the wild-type and experimental groups failed the F test, pairwise heteroscedastic T-tests were performed using Excel and StatPlus:mac (AnalystSoft). To construct box plots, standard box plot conventions were used. The first (Q1) and third (Q3) quartiles, interquartile range (IQR = Q3 - Q1) and mean were calculated. Extreme outliers were defined as lying beyond the outer fences OF1 = Q1 - 3 * IQR and OF2 = Q3 + 3 * IQR. Mild outliers were defined as lying between OF1 and Q1- 1.5 * IQR or OF2 and Q3 + 1.5 * IQR. Box plots were constructed using StatPlus:mac.

For analysis of *let-502(ts)* embryos, worms carrying embryos were shifted to an intermediate, restrictive temperature (25.5°C) and grown overnight. Embryos were recovered, stained via freeze-cracking [10] using MH27 and anti-UNC-94 antibodies and appropriate secondary antibodies (1:50 α-rabbit-FITC, 1:50 α-mouse-Texas Red), and imaged using spinning disc confocal microscopy. The thickness of the junctional proximal actin at dorsal::seam boundaries was measured at several points along the perimeter of individual cells using ImageJ (available at http://rsbweb.nih.gov/ij/), and an average thickness was calculated for each cell measured. The length/width ratio of each cell was also measured in ImageJ using the AJM-1 signal. The resulting actin band thickness vs. length/width data were plotted in Excel and a curve fit was obtained using a power law.

Coimmunoprecipitation Assays

Embryos were collected from 10 large plates grown for 3-4 days at 20°C, homogenized in Lysis buffer + 0.25% Triton X-100, subjected to centrifugation to clear the lysates, and precleared by incubation on ice with 20µl of a 50% slurry of Protein G-Agarose beads essentially as described [13, 14]. To perform IPs, 5µl E36 mouse monoclonal anti-GFP (Invitrogen) was added to pre-cleared lysate and rotated at 4°C for 1 hour, 40ul of 50% prepared Protein G-Agarose bead slurry (Pierce)

was added, and rotated again at 4°C for 1 hour. Beads were sedimented at 3000 rpm for 3 min (4°C), washed 3X with Lysis buffer, and 25ul 4x SDS-PAGE sample buffer was then added to preclear, prewash, and IP bead fractions on ice. Collected samples were then subjected to SDS-PAGE on an 8% gel, along with 10 μl of Precision Plus Kaleidoscope Standard (Bio-Rad), and blotted onto PVDF membrane. Blots were blocked using TBST + 5% non-fat dry milk, incubated in 1:2500 primary (anti-UNC-94) antibody, washed in TBST, incubated in 1:10,000 anti-Rabbit HRP conjugate, and visualized using enhanced chemiluminescence (ECL; Pierce) on X-ray film.

Expression and Purification of Recombinant UNC-94 Protein

A full-length *unc-94b* cDNA was cloned into plasmid pKLD37 using a vector provided by I. Rayment (Dept. of Biochemistry, Univ. of Wisconsin), which consisted of pET31b with an N-term 6His-rTEV site. The *Escherichia coli* strain BL21 (DE3) was transformed with the expression vector and cultured in M9ZB medium (Novagen, EMD Biosciences, Inc., San Diego, CA) containing 50 μg/ml ampicillin at 37 °C until A_{600} reached 0.6 cm^{-1}. Protein expression was induced by adding 0.4 mM IPTG for 3 hours. The cells were harvested by centrifugation at 5,000 *g* for 10 minutes and disrupted by a French Pressure cell at 360-580 kg/cm^2 in a buffer containing 0.3 M NaCl, 50 mM $NaPO_4$, 10 mM imidazole, 1 mM phenylmethanesulfonyl fluoride, pH 7.4. The homogenates were centrifuged at 20,000 *g* and the supernatants applied to a TALON cobalt affinity column (Clontech, Mountain View, CA). Bound proteins were eluted with 0.3 M NaCl, 50 mM $NaPO_4$, 100 mM imidazole, pH 7.4. The fractions containing UNC-94 were dialyzed against 10 mM PIPES, 0.2 mM dithiothreitol, pH 7.0 and purified further with a Mono-Q column (Amersham Biosciences, GE Healthcare Bio-sciences, Corp., Piscataway, NJ) by elution with a linear NaCl gradient (0.1-0.5 M). Fractions containing purified UNC-94 were dialyzed against F-buffer (0.1 M KCl, 2 mM $MgCl_2$, 1 mM dithiothreitol, 20 mM Hepes-NaOH, pH 7.5). Concentrations of UNC-94 were determined by densitometry of Coomassie blue-stained protein bands after SDS-PAGE using actin as a standard.

Actin Bundling Assays

Recombinant UNC-94 was expressed and purified as described above. GST-tagged HMP-1 was produced using constructs previously described [4], purified on glutathione beads, eluted with 10 mM glutathione, and cleaved with TEV protease in 50 mM Tris, pH 8 in solution. The digest was purified using a Sephacryl S-300 column. Rabbit muscle G-actin (20% labeled with DyLight549) [15] was polymerized in the presence of chicken CapZ [16] at a 100:1 molar ratio. Filaments were diluted to 5 μM actin with or without 5 μM HMP-1 and 2.5 μM UNC-94 and incubated for 15 min, mounted on nitrocellulose-coated coverslips, and observed by epifluorescence using a Nikon TE2000 inverted

microscope. The curvilinear lengths of resulting bundles were measured using the NeuronJ plugin for ImageJ, available at http://rsbweb.nih.gov/ij/. Statistics were performed using Excel and StatPlus:Mac.

Supplemental References

1. Pettitt, J., Cox, E.A., Broadbent, I.D., Flett, A., and Hardin, J. (2003). The Caenorhabditis elegans p120 catenin homologue, JAC-1, modulates cadherin-catenin function during epidermal morphogenesis. J Cell Biol *162*, 15-22.
2. Diogon, M., Wissler, F., Quintin, S., Nagamatsu, Y., Sookhareea, S., Landmann, F., Hutter, H., Vitale, N., and Labouesse, M. (2007). The RhoGAP RGA-2 and LET-502/ROCK achieve a balance of actomyosin-dependent forces in C. elegans epidermis to control morphogenesis. Development *134*, 2469-2479.
3. Boulin, T., Etchberger, J.F., and Hobert, O. (2006). Reporter gene fusions. WormBook, 1-23.
4. Kwiatkowski, A.V., Maiden, S.L., Pokutta, S., Choi, H.J., Benjamin, J.M., Lynch, A.M., Nelson, W.J., Weis, W.I., and Hardin, J. (2010). In vitro and in vivo reconstitution of the cadherin-catenin-actin complex from Caenorhabditis elegans. Proc Natl Acad Sci U S A *107*, 14591-14596.
5. Stevenson, T.O., Mercer, K.B., Cox, E.A., Szewczyk, N.J., Conley, C.A., Hardin, J.D., and Benian, G.M. (2007). unc-94 encodes a tropomodulin in Caenorhabditis elegans. Journal of molecular biology *374*, 936-950.
6. Fraser, A.G., Kamath, R.S., Zipperlen, P., Martinez-Campos, M., Sohrmann, M., and Ahringer, J. (2000). Functional genomic analysis of C. elegans chromosome I by systematic RNA interference. Nature *408*, 325-330.
7. Brenner, S. (1974). The genetics of Caenorhabditis elegans. Genetics *77*, 71-94.
8. Timmons, L., and Fire, A. (1998). Specific interference by ingested dsRNA. Nature *395*, 854.
9. Sheffield, M., Loveless, T., Hardin, J., and Pettitt, J. (2007). C. elegans Enabled exhibits novel interactions with N-WASP, Abl, and cell-cell junctions. Curr Biol *17*, 1791-1796.
10. Williams-Masson, E.M., Malik, A.N., and Hardin, J. (1997). An actin-mediated two-step mechanism is required for ventral enclosure of the C. elegans hypodermis. Development *124*, 2889-2901.
11. Costa, M., Raich, W., Agbunag, C., Leung, B., Hardin, J., and Priess, J.R. (1998). A putative catenin-cadherin system mediates morphogenesis of the Caenorhabditis elegans embryo. J Cell Biol *141*, 297-308.
12. Simske, J.S., Koppen, M., Sims, P., Hodgkin, J., Yonkof, A., and Hardin, J. (2003). The cell junction protein VAB-9 regulates adhesion and epidermal morphology in C. elegans. Nat Cell Biol *5*, 619-625.
13. Bernadskaya, Y.Y., Patel, F.B., Hsu, H.T., and Soto, M.C. (2011). Arp2/3 promotes junction formation and maintenance in the Caenorhabditis elegans intestine by regulating membrane association of apical proteins. Molecular biology of the cell *22*, 2886-2899.
14. Giuliani, C., Troglio, F., Bai, Z., Patel, F.B., Zucconi, A., Malabarba, M.G., Disanza, A., Stradal, T.B., Cassata, G., Confalonieri, S., et al. (2009). Requirements for F-BAR proteins TOCA-1 and TOCA-2 in actin dynamics and membrane trafficking during Caenorhabditis elegans oocyte growth and embryonic epidermal morphogenesis. PLoS genetics *5*, e1000675.
15. Liu, Z., Klaavuniemi, T., and Ono, S. (2010). Distinct roles of four gelsolin-like domains of Caenorhabditis elegans gelsolin-like protein-1 in actin filament severing, barbed end capping, and phosphoinositide binding. Biochemistry *49*, 4349-4360.
16. Soeno, Y., Abe, H., Kimura, S., Maruyama, K., and Obinata, T. (1998). Generation of functional beta-actinin (CapZ) in an E. coli expression system. J Muscle Res Cell Motil *19*, 639-646.